Journal of Southeast University (English Edition) Vol. 39, No. 3, pp. 225 - 232 Sept. 2023 ISSN 1003—7985

Vibration analysis of circular Janus MoSSe plates

Liu Xinjie Wang Lifeng

(State Key Laboratory of Mechanics and Control for Aerospace Structures, Nanjing University of Aeronautics and Astronautics, Nanjing 210016, China)

Abstract: The vibration behavior of Janus monolayer molybdenum sulfoselenide (MoSSe) was studied based on molecular dynamics (MD) simulations and the finite element method (FEM). MoSSe plates were simulated by FEM through the incorporation of intrinsic strain caused by lattice mismatch to the double-layer plate model. The vibrations of circular MoSSe plates with free boundaries and a clamped edge were determined by MD simulations and FEM. In addition, the effects of plate size, strain, and pressure on the natural frequency of the plates were investigated. The results showed that the natural frequency of the circular MoSSe plate with free boundaries gradually decreased with increasing plate size. Furthermore, a significant discontinuity in frequency was observed due to bowl and tube warpage when the diameter reached 8.6 nm. The MD simulation and FEM calculation results were consistent in terms of the natural frequencies of the circular MoSSe plates of different sizes. In addition, the effects of strain and pressure on the natural frequency determined by the two methods were consistent for small deformations. The vibration of the MoSSe plate could be well predicted by the double-layer plate model.

Key words: Janus monolayer molybdenum sulfoselenide (MoSSe); molecular dynamics (MD); warpage; natural frequency

DOI: 10.3969/j.issn.1003 - 7985.2023.03.002

Since the discovery of graphene, two-dimensional (2D) materials have attracted considerable research attention owing to their remarkable mechanical, electronic, and thermal properties [1-8]. In addition to graphene, 2D transition-metal dichalcogenides (TMDs) [9-12] have garnered considerable attention owing to their unique physical and chemical properties. The mechanical, electrical, optical, and thermal properties of molybdenum disulfide (MoS_2), a typical TMD material, have been extensively explored[13-16]. In recent years, 2D heterostructures composed of vertically stacked 2D materials with distinct properties have exhibited novel characteristics[17-18]. Molybdenum sulfoselenide (MoSSe) possesses a structure similar to heterostructures, even though it is composed of a single material. In a recent study, Lu et al. [19] completely replaced the top-layer S atoms in MoS_2 with Se atoms. The Janus structure of MoSSe was confirmed through scanning transmission electron microscopy and energy-dependent X-ray photoelectron spectroscopy. The presence of vertical dipoles was confirmed through second harmonic generation and piezoresponse force microscopy measurements. Zhang et al. [20] controlled the sulfide action to replace the top Se atoms of monolayer molybdenum diselenide ($MoSe_2$) with S atoms, while the bottom layer of Se atoms remained unaffected. Through this method, a Janus monolayer MoSSe structure was formed, comprising three layers of atoms from top to bottom, namely sulfur, molybdenum, and selenium. Idrews et al. [21] used hybrid density-functional theory calculations to investigate Janus monolayers and their associated van der Waals heterojunctions. They discovered that MoSSe is a direct-bandgap semiconductor. Indirect-bandgap semiconductors can be converted into direct-bandgap counterparts using external electric fields. In direct-bandgap semiconductors, electrons can directly excite or de-excite by the absorption or emission of photons with no involvement of phonons in the processes. This property renders them more suitable for manufacturing optoelectronic devices. Dong et al. [22] investigated the planar and vertical piezoelectric properties of monolayer and multilayer MXY structures (where M = Mo or W, and X/Y = S, Se, or Te) based on ab initio calculations. Under substrate influence, uniaxially strained MXY structures exhibited high in-plane piezoelectric polarization but significantly weaker out-of-plane piezoelectric polarization. Conversely, laterally strained multilayer MXY structures exhibited substantial out-of-plane piezoelectric polarization. These studies highlighted the applicability of MXY structures in smart nanodevice applications. Kandemir et al. [23] employed first-principle computations to investigate the structural and phononic properties of MoSSe monolayers. They utilized out-of-plane anisotropy to demonstrate the unique vertical pressure effect on the vibrational characteristics of Janus materials due to the asymmetric structure of Janus MoSSe monolayers. Pham et al. [24] developed ultrathin graphene/MoSeS and graphene/MoSSe

Received 2023-05-19, **Revised** 2023-08-01.

Biographies: Liu Xinjie (1998—), male, Ph. D. candidate; Wang Lifeng (corresponding author), male, doctor, professor, walfe@nuaa.edu.cn.

Foundation items: The National Natural Science Foundation of China (No. 51921003), the National Science Fund for Distinguished Young Scholars (No. 11925205).

Citation: Liu Xinjie, Wang Lifeng. Vibration analysis of circular Janus MoSSe plates[J]. Journal of Southeast University (English Edition), 2023, 39(3): 225 - 232. DOI: 10.3969/j.issn.1003 - 7985.2023.03.002.

heterostructures and studied their structural and electrical properties and the effect of vertical electric fields on these heterostructures. These designed heterostructures were intended for applications in nanoelectronic and optoelectronic devices.

Studying the vibration of nanoscale structures is imperative owing to the crucial role of vibration behavior in the functionality of smart nanodevices. Jiang et al. [25] investigated the nanomechanics and vibration behavior of graphene sheets, employing a 2D plate model that accounted for varying sizes and boundary conditions. The simulation results highlighted the accuracy and efficiency of the 2D plate model, demonstrating its potential as a promising alternative for modeling nanomechanics and analyzing the vibration of graphene sheets when compared with several well-established experiments and equivalent theoretical models. Akgöz et al. [26] investigated the free vibration of a single-layered graphene sheet positioned on an elastic matrix. They derived the governing equation of motion using the thin plate theory in conjunction with Hamilton's principle. Kitipornchai et al. [27] employed a continuum model to assess the vibration of multilayered graphene sheets, revealing that varying the number of layers can lead to various resonance modes. Zhang et al. [28] explored the vibration frequency of rippled single-layered graphene sheets and identified that introducing functional groups, defects, carbon nanotubes, and surface wrinkles can induce significant frequency shifts in pristine single-layered graphene sheets. Zhang et al. [29] investigated the thermal vibration of rectangular monolayer black phosphorus based on an orthotropic plate model and molecular dynamics (MD) simulations. MD simulations and the orthotropic plate model, combined with the law of energy equipartition, provided insights into the root-mean-square amplitude of rectangular monolayer black phosphorus. Through MD simulations and a continuous plate model, Yi et al. [30] investigated the vibration behavior of single-layered hexagonal boron nitride and explored the effect of an electric field on the intrinsic frequency. Zhang et al. [31] employed the circular Mindlin plate model to analyze the vibration of circular single-layered MoS_2. The findings indicated that for very small plate sizes, particularly at higher-order frequencies, the natural frequencies computed by the Mindlin plate model aligned more closely with those determined by the MD method than those computed by the Kirchhoff plate model. Thus, it is necessary to reveal the dynamic behavior of the Janus monolayer MoSSe structure.

To the best of our knowledge, the vibration behavior of Janus MoSSe has not been studied yet. Therefore, MD simulations and the finite element method (FEM) are employed to investigate the vibrations of Janus monolayer MoSSe, considering free-boundary and clamped-edge conditions. In addition, the effects of size and the initial stress are studied.

1 Vibration Analysis of the MoSSe Plate with MD Simulation

The atomic structure of Janus monolayer MoSSe features a sandwich-like arrangement with selenium, molybdenum, and sulfur atoms spanning from the upper to lower layers (see Fig. 1). The Stillinger-Weber (SW) potential, recently formulated for various MX_2 structures (M = Mo, W; X = S, Se, Mo) and their alloys and lateral heterostructures, is adopted here [32]. Thus, the interatomic interactions within the Janus monolayer MoSSe are described using the SW potential function.

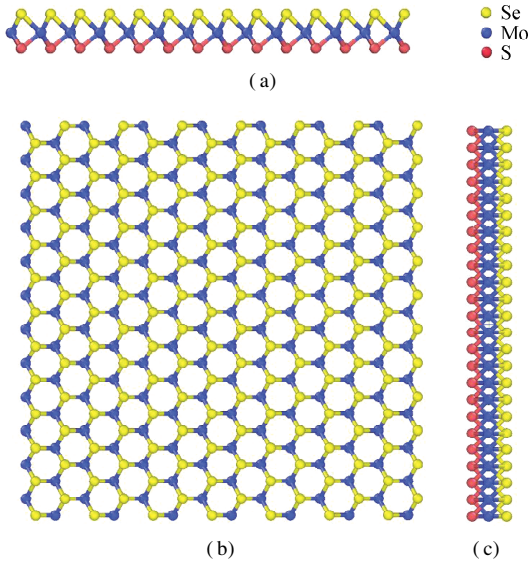

Fig. 1 Atomic structure of the Janus monolayer molybdenum sulfoselenide (MoSSe) structure. (a) Side view along the armchair direction; (b) Top view; (c) Side view along the zigzag direction

The mechanical properties of the monolayer in the zigzag and armchair directions are determined through MD simulations using a square sheet under periodic boundary conditions; the monolayer thickness is set at 0.324 nm. The model is subjected to stretching along a single direction, and during this process, stresses in the tensile direction and strains in the nontensile direction are recorded. The resulting stress-strain curves for the armchair and zigzag directions are shown in Fig. 2(a). The red solid line represents the stress-strain curve for stretching along the armchair direction, while the black dashed line corresponds to stretching along the zigzag direction. The relationship between strains along the armchair and zigzag directions during uniaxial tension is shown in Fig. 2(b). The red curve shows the relationship between the zigzag-direction strain (vertical coordinate) and armchair-direction strain (horizontal coordinate) during stretching along the armchair direction. Furthermore, the black curve shows the relationship between the armchair-direction strain (vertical coordinate) and zigzag-direction strain (horizontal coordinate) during stretching along the zigzag direction. Within the linear range, stresses in both direc-

tions exhibit nearly identical behavior at equal strains. For small tensile strains, Poisson's ratio values are almost identical for both directions. For simplicity, the material can be treated as isotropic. Young's modulus is taken as the average of the two directions, yielding 230.4 GPa, and Poisson's ratio is similarly averaged at 0.23.

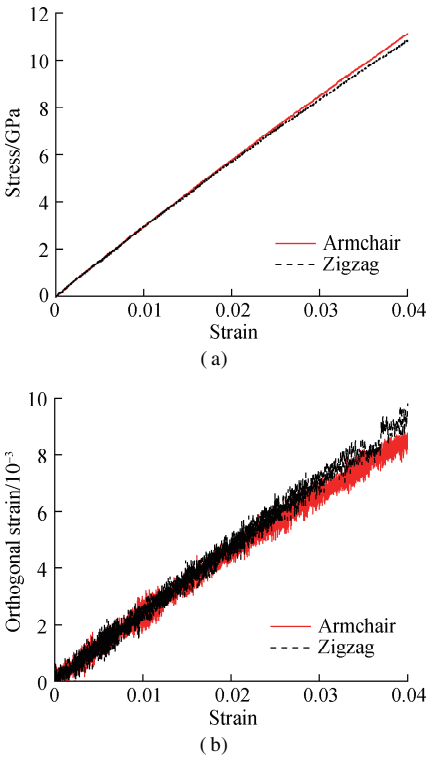

Fig. 2 Static characteristic curves. (a) Stress-strain curve; (b) Strain curve in two orthogonal directions

The natural frequencies of the circular MoSSe plate with a clamped edge and free boundaries can be determined using the MD software Large-scale Atomic/Molecular Massively Parallel Simulator [33]. Initially, the boundaries of the MoSSe plate are set as free boundaries. The equilibrium state of the structure is achieved by the steepest descent method combined with the conjugate gradient approach for energy minimization. Thereafter, MD simulations are performed using the NVT ensemble, and a temperature of 300 K is maintained using a Nose-Hoover thermostat with a time step of 1 fs for 5 ns. During the calculation related to the free-boundary case, the linear and angular momentums of the model are constrained to zero to avoid rigid-body displacements. The positions of the selected MoSSe atoms are recorded at every 100 steps. Subsequently, vibrational frequencies are computed by fast Fourier transformation (FFT). Fig. 3(a) shows the out-of-plane displacement of a sulfur atom selected from the MoSSe circular plate with a clamped edge. The thermal vibrational spectrum corresponding to the atom's displacement derived by FFT is shown in Fig. 3(b). Each peak in the spectrum represents a natural frequency of the MoSSe plate. In addition, the figure shows the vibration modes obtained by MD simulation. A periodic force is applied to the MoSSe plate with a frequency similar to the plate's natural frequency. Once a steady state is reached, vibration modes corresponding to the natural frequency can be observed.

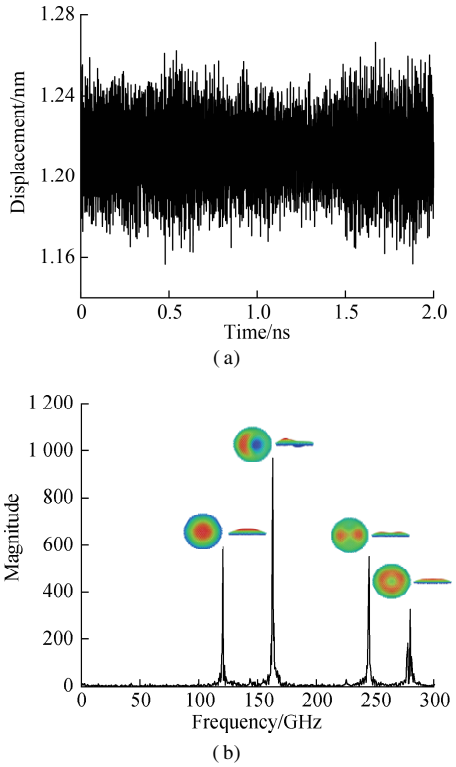

Fig. 3 Atomic out-of-plane displacements and the vibration spectrum of the molybdenum sulfoselenide circular plate with a diameter of 7.5 nm after warpage. (a) Atomic displacement (z-coordinate); (b) Vibration spectrum and modes obtained by MD simulation

During computations with free-boundary conditions, with the increasing diameter of the circular plate, the natural frequencies of each order gradually decrease while maintaining a relatively continuous trend. However, a discontinuity arises when the diameter reaches 8.6 nm (see Fig. 4). The MD simulation reveals alterations in the morphology of the MoSSe plate after relaxation. As

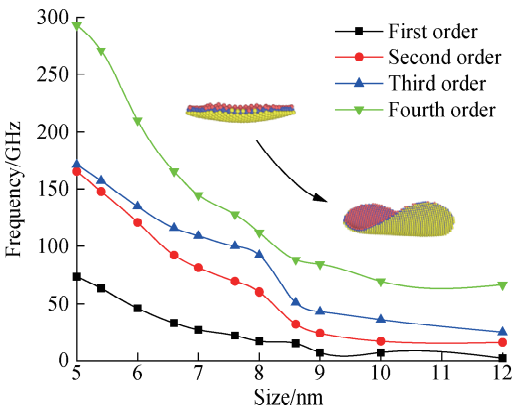

Fig. 4 First- to fourth-order natural frequencies of molybdenum sulfoselenide circular plates with different diameters

the model size increases, the warping transforms from a uniformly curved bowl shape into a tubular structure with warped ends, and the extent of warping intensifies. The MD simulation results indicate that at a diameter of 8.6 nm, a shift from bowl-like warping to tubular warping occurs. For diameters greater than 9.0 nm, a complete transition to tubular warping occurs. To validate the rationality of this outcome, a continuous medium model is employed to simulate the MoSSe plate, and its vibration frequency is computed for comparison with the MD simulation results.

2 Continuum Mechanics Model for Vibration of the MoSSe plate

From the calculations discussed in the previous section, a discontinuity is observed in the natural frequencies of the MoSSe circular plate with free boundaries. Furthermore, two distinct warping morphologies, bowl and tubular warping, are identified. FEM analysis is conducted to investigate the vibration behavior of the MoSSe plates. For meshing, a free tetrahedral mesh is used. Convergence results are achieved with regular or high meshing densities, where the minimum cell size is set to 0.04 nm, maximum cell size to 0.55 nm, and maximum cell growth rate to 1.4. A circular composite plate comprising of two sublayers is used to analyze the warpage of the Janus monolayer MoSSe structure. These two sublayers are closely integrated, forming a unified structure. The upper layer represents the molybdenum-selenide structure, with a thickness of 0.171 nm, while the lower layer represents the molybdenum-sulfur structure, with a thickness of 0.153 nm. The strains due to lattice mismatch ($\varepsilon_{\text{Mo-S}} = (\alpha_{\text{MoS}_2} - \alpha_{\text{MoSSe}})/\alpha_{\text{MoS}_2}$, $\varepsilon_{\text{Mo-Se}} = (\alpha_{\text{MoSe}_2} - \alpha_{\text{MoSSe}})/\alpha_{\text{MoSe}_2}$) are incorporated into the corresponding sublayer as the initial state[34–39], where $\varepsilon_{\text{Mo-S}}$ and $\varepsilon_{\text{Mo-Se}}$ represent the strains in the Mo-S layer and Mo-Se layers, respectively, and α_{MoSSe}, α_{MoS_2}, and α_{MoSe_2} represent the lattice constants of monolayers MoSSe, MoS_2, and $MoSe_2$, respectively; the relevant parameters are listed in Tab. 1. After warpage, the natural frequencies of the plates with different boundary conditions are calculated. The FEM calculation results show identical transformations of the warpage morphology (see Fig. 5). Both methods yield the same warpage patterns and dimensions of warpage-pattern changes, which verifies the rationality of the model. The natural frequencies of the plates with free boundaries calculated by these two methods are shown in Fig. 6. The first four natural frequencies obtained by both methods decrease with increasing plate size. When the diameter of the MoSSe circular plate reaches 7 nm, the second- and third-order frequencies obtained by FEM overlap.

Tab. 1 Material parameters

Material	α/nm	$h_{\text{Mo-S}}$/nm	$h_{\text{Mo-Se}}$/nm	$l_{\text{Mo-S}}$/nm	$l_{\text{Mo-Se}}$/nm	θ/(°)
MoSSe	0.323	0.153	0.171	0.241	0.258	81.428
MoS_2	0.320	0.158		0.242		
$MoSe_2$	0.329		0.172		0.253	

Notes: α represents the lattice constant; $h_{\text{Mo-S}}$ and $h_{\text{Mo-Se}}$ represent the heights of the Mo-S and Mo-Se layers, respectively; $l_{\text{Mo-S}}$ and $l_{\text{Mo-Se}}$ represent the bond lengths of Mo-S and Mo-Se, respectively; θ represents the bond angle ∠S-Mo-Se of the Janus MoSSe structure.

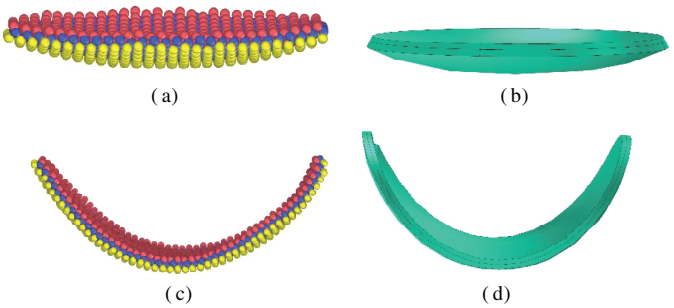

Fig. 5 Molecular dynamics (MD) simulation and finite element method (FEM) analysis results for the warpage of circular molybdenum sulfoselenide plates with diameters of 8-14 nm. (a) MD results with diameters of 8 nm; (b) FEM results with diameters of 8 nm; (c) MD results with diameters of 14 nm; (d) FEM results with diameters of 14 nm

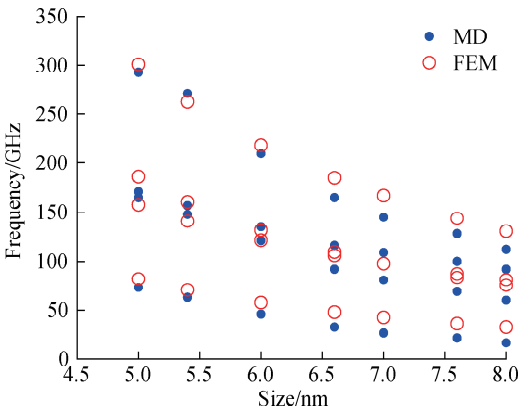

Fig. 6 First- to fourth-order natural frequencies of the molybdenum sulfoselenide shallow spherical shell with free boundaries

The warpage morphologies change when the diameter of the circular plate reaches 8.6 nm, similar to the calculation results with free-boundary conditions. To analyze circular plates with clamped edges, the diameter is maintained at <8.6 nm to ensure the persistence of bowl-like warping. The calculation results of the first eight natural frequencies of the shallow spherical shell, which is formed by warping a circular plate with a diameter of 7.5 nm, are shown in Fig. 7. The frequencies obtained by the two methods are consistent. Furthermore, the vibration modes are obtained by FEM.

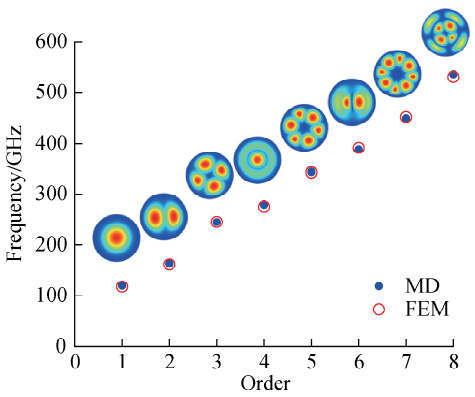

Fig. 7 First eight natural frequencies and modes of the shallow spherical shell formed by warping the circular plate of the Janus MoSSe structure with a diameter of 7.5 nm

To further investigate the effect of plate size on the vibration frequency, circular plate models of MoSSe with diameters of 4.5 to 8.1 nm are established. The natural frequencies of the MoSSe plates with clamped edges are shown in Fig. 8. The natural frequency decreases with the increasing diameter of the shallow spherical shell. Furthermore, the discrepancy between the results obtained by the two methods decreases with increasing plate size. Overall, the two methods provide consistent results, and the double-layer plate model can well predict the warpage and natural frequency of the MoSSe circular plate.

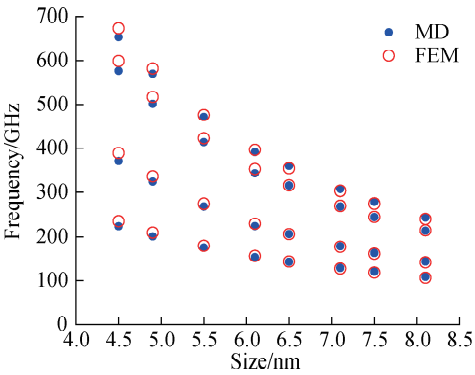

Fig. 8 First- to fourth-order natural frequencies of the molybdenum sulfoselenide shallow spherical shell with a clamped edge

3 Vibration Analysis of the Circular MoSSe Plate with Initial Stress

In this section, the effect of the initial stress on the natural frequency of the MoSSe circular plate after the warpage is investigated.

To analyze the effect of tension on the vibration of the Janus MoSSe structure, a MoSSe plate model with a diameter of 7.5 nm under different strains was established. Thereafter, uniaxial and radial stretching cases were investigated. Uniaxial stretching was performed along the armchair and zigzag directions (see Fig. 9(a)). The natural frequencies of the MoSSe plate with a clamped edge after uniaxial stretching are shown in Fig. 9(b). A new frequency emerges from the original second-order frequency due to the asymmetry introduced by the strain in the two orthogonal directions. In the unstretched case, the properties along the zigzag and armchair directions exhibit similarity. Therefore, the second-order frequencies corresponding to the zigzag and armchair directions are the same. However, stretching induces an asymmetry between these orthogonal directions, leading to differences in natural frequencies. Thus, the original second-order frequency splits into a lower and higher natural frequency. The difference between the second- and third-order frequencies gradually increases with increasing strain. Furthermore, the fourth-order frequency also gradually increases, but the first-order frequency decreases until the strain reaches 0.04 and then gradually increases. Stretching along the armchair and zigzag directions yields the same effects on the natural frequency. Fig. 10 shows the effect of radial stretching on the natural frequency. The first-order frequency decreases until the strain reaches 0.15 and then gradually increases, and higher-order frequencies increase as the strain increases. Although the same trend is observed in the FEM calculations, the consistency between the two results is predominantly maintained only when the strain is small. For larger strains, the frequencies determined by FEM increase at a higher rate than that determined by MD, and when the strain reaches 0.03, a substantial discrepancy exists between the two results.

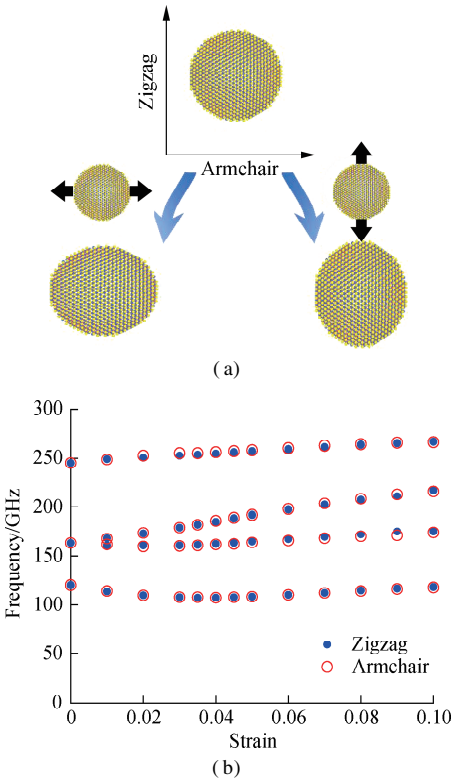

Fig. 9 Effect of uniaxial stretching on the natural frequency. (a) Stretching in two directions; (b) Natural frequencies of the molybdenum sulfoselenide plate with a clamped edge after uniaxial stretching

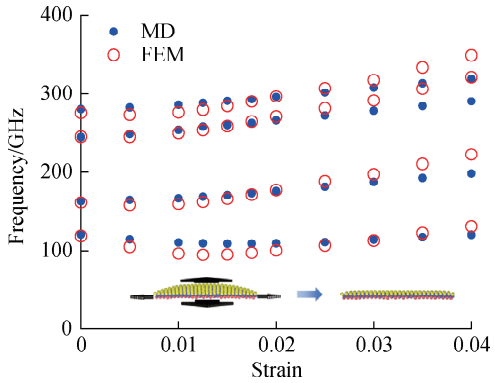

Fig. 10 Effect of radial stretching on the natural frequency

Finally, the effect of pressure on the natural frequency is investigated. The boundary of the plate is fixed after sufficient warping before pressure application. The frequency obtained by the MD simulation dramatically increases in the pressure range of −0.073 to 0.146 GPa and slowly increases for pressure greater than 0.146 GPa (see Fig. 11). When the pressure value is positive, the pressure aligns with the upward direction in Fig. 11, and when the value is negative, the pressure aligns with the downward direction. Under low pressure values, the results obtained by the two methods are consistent, and under large pressure values, a substantial discrepancy occurs between the two results.

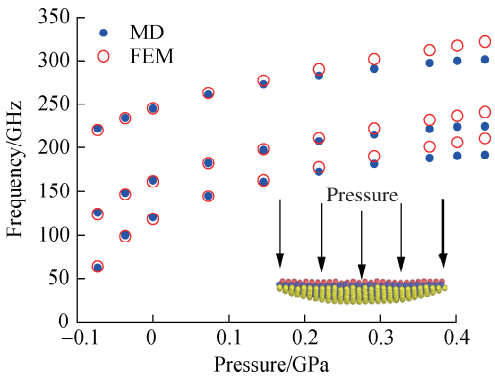

Fig. 11 First three natural frequencies of the molybdenum sulfoselenide shallow spherical shell with z-directional pressure

4 Conclusions

1) The analysis of vibrations in the MoSSe circular plate with free boundaries reveals a distinct frequency discontinuity. This phenomenon is associated with the presence of two warpage patterns, a finding that is successfully reproduced in FEM calculations.

2) The natural frequencies of the MoSSe circular plate with a clamped edge obtained by the MD method and FEM are consistent. The discrepancies between the results of these two methods decrease with the increasing size of the MoSSe structure. The comparison reveals that the vibrations of the circular MoSSe plate are well predicted by the double-layer model.

3) The effects of strain and pressure on the natural frequency are also investigated. The frequencies obtained by FEM and the MD simulation are consistent under sufficiently small deformations. However, under larger deformations, the frequencies determined by FEM are higher than those determined by the MD simulation.

References

[1] Novoselov K S, Geim A K, Morozov S V, et al. Electric field effect in atomically thin carbon films[J]. *Science*, 2004, **306**(5696): 666−669. DOI: 10.1126/science.1102896.

[2] Lee C, Wei X, Kysar J W, et al. Measurement of the elastic properties and intrinsic strength of monolayer graphene[J]. *Science*, 2008, **321**(5887): 385−388. DOI: 10.1126/science.1157996.

[3] Galashev A Y, Vorob'ev A S. An ab initio study of the interaction of graphene and silicene with one-, two-, and three-layer planar silicon carbide[J]. *Physica E*: *Low-Dimensional Systems and Nanostructures*, 2022, **138**: 115120. DOI: 10.1016/j.physe.2021.115120.

[4] Yan J W, Zhu J H, Li C, et al. Decoupling the effects of material thickness and size scale on the transverse free vibration of BNNTs based on beam models[J]. *Mech Syst Signal Pr*, 2022, **166**: 108440. DOI: 10.1016/j.ymssp.2021.108440.

[5] Yan J W, Zhang W, Lai S K, et al. Large amplitude vibration and bistable jump of functionally graded graphene-platelet reinforced porous composite plates [J/OL]. *Waves in Random and Complex Media*. (2022-11-12)[2023-04-08]. https://doi.org/10.1080/17455030.2022.2141915.

[6] Wu J W, Tao Y, Chen C, et al. Molecular dynamics simulations of strain-dependent thermal conductivity of single-layer black phosphorus[J]. *Journal of Southeast University* (*English Edition*), 2018, **34**(1): 43−47. DOI: 10.3969/j.issn.1003-7985.2018.01.007.

[7] Chen C, Chen Y F, Sha J J, et al. Molecular dynamics simulation of ion transportation through graphene nanochannels[J]. *Journal of Southeast University* (*English Edition*), 2017, **33**(2): 171−176. DOI: 10.3969/j.issn.1003-7985.2017.02.008.

[8] Yan J W, Zhang W. An atomistic-continuum multiscale approach to determine the exact thickness and bending rigidity of monolayer graphene[J]. *Journal of Sound and Vibration*, 2021, **514**: 116464. DOI: 10.1016/j.jsv.2021.116464.

[9] Deng S, Li L, Li M. Stability of direct band gap under mechanical strains for monolayer MoS_2, $MoSe_2$, WS_2 and WSe_2[J]. *Physica E*: *Low-dimensional Systems and Nanostructures*, 2018, **101**: 44−49. DOI: 10.1016/j.physe.2018.03.016.

[10] Song Z, Schultz T, Ding Z, et al. Electronic properties of a 1D intrinsic/p-doped heterojunction in a 2D transition metal dichalcogenide semiconductor[J]. *ACS Nano*,

2017, **11**(9): 9128 − 9135. DOI: 10.1021/acsnano.7b03953.

[11] Wierzbowski J, Klein J, Sigger F, et al. Direct exciton emission from atomically thin transition metal dichalcogenide heterostructures near the lifetime limit[J]. *Scientific Reports*, 2017, **7**: 12383. DOI: 10.1038/s41598-017-09739-4.

[12] Najam F, Tan M L P, Ismail1 R, et al. Two-dimensional (2D) transition metal dichalcogenide semiconductor field-effect transistors: The interface trap density extraction and compact model[J]. *Semiconductor Science and Technology*, 2015, **30**: 075010. DOI: 10.1088/0268-1242/30/7/075010.

[13] Salih E, Ayesh A I. First principle study of transition metals codoped MoS_2 as a gas sensor for the detection of NO and NO_2 gases[J]. *Physica E: Low-dimensional Systems and Nanostructures*, 2021, **131**: 114736. DOI: 10.1016/j.physe.2021.114736.

[14] Xiong Q L, Kitamura T, Li Z H. Crystal orientation-dependent mechanical property and structural phase transition of monolayer molybdenum disulfide[J]. *Journal of Applied Physics*, 2017, **122**: 135105. DOI: 10.1063/1.4996941.

[15] Yasaei P, Foss C J, Karis K, et al. Interfacial thermal transport in monolayer MoS_2- and graphene-based devices [J]. *Advanced Materials Interfaces*, 2017, **4**(17): 1700334. DOI: 10.1002/admi.201700334.

[16] Nguyen C V, Hieu N N, Poklonski N A, et al. Magneto-optical transport properties of monolayer MoS_2 on polar substrates[J]. *Physical Review B*, 2017, **96**(12): 125411. DOI: 10.1103/PhysRevB.96.125411.

[17] Zhang Y Q, Wang L F, Jiang J N. Thermal vibration of MoS_2/black phosphorus bi-layered heterostructure [J]. *Physica E: Low-dimensional Systems and Nanostructures*, 2019, **114**: 113597. DOI: 10.1016/j.physe.2019.113597.

[18] Novoselov K S, Mishchenko A, Carvalho A, et al. 2D materials and van der Waals heterostructures[J]. *Science*, 2016, **353**(6298): aac9439. DOI: 10.1126/science.aac9439.

[19] Lu A Y, Zhu H Y, Xiao J, et al. Janus monolayers of transition metal dichalcogenides[J]. *Nature Nanotechnology*, 2017, **12**: 744 − 749. DOI: 10.1038/nnano.2017.100.

[20] Zhang J, Jia S, Kholmanov I, et al. Janus monolayer transition-metal dichalcogenides[J]. *ACS Nano*, 2017, **11**(8): 8192 − 8198. DOI: 10.1021/acsnano.7b03186.

[21] Idrews M, Din H U, Ali R, et al. Optoelectronic and solar cell applications of Janus monolayers and their van der Waals heterostructures[J]. *Physical Chemistry Chemical Physics*, 2019, **21**: 18612 − 18621. DOI: 10.1039/c9cp02648g.

[22] Dong L, Lou J, Shenoy V B. Large in-plane and vertical piezoelectricity in Janus transition metal dichalchogenides [J]. *ACS Nano*, 2017, **11**(8): 8242 − 8248. DOI: 10.1021/acsnano.7b03313.

[23] Kandemir A, Peeters F M, Sahin H. Monitoring the effect of asymmetrical vertical strain on Janus single layers of MoSSe via vibrational spectrum[J]. *The Journal of Chemical Physics*, 2018, **149**: 084707. DOI: 10.1063/1.5043207.

[24] Pham K D, Hieu N N, Phuc H V, et al. First principles study of the electronic properties and schottky barrier in vertically stacked graphene on the Janus MoSeS under electric field [J]. *Computational Materials Science*, 2018, **153**: 438 − 444. DOI: 10.1016/j.commatsci.2018.07.017.

[25] Jiang S W, Shi S, Wang X F. Nanomechanics and vibration analysis of graphene sheets via a 2D plate model [J]. *J Phys D: Appl Phys*, 2014, **47**(4): 045104. DOI: 10.1088/0022-3727/47/4/045104.

[26] Akgöz B, Civalek Ö. Free vibration analysis for single-layered graphene sheets in an elastic matrix via modified couple stress theory[J]. *Materials & Design*, 2012, **42**: 164 − 171. DOI: 10.1016/j.matdes.2012.06.002.

[27] Kitipornchai S, He X Q, Liew K M. Continuum model for the vibration of multilayered graphene sheets [J]. *Phys Rev B*, 2005, **72**: 075443. DOI: 10.1103/PhysRevB.72.075443.

[28] Zhang Z Y, Lan L, Wang Y F, et al. Vibration frequency analysis of rippled single-layered graphene sheet: Toward the nano resonant devices design[J]. *Physica E: Low-dimensional Systems and Nanostructures*, 2019, **114**: 113580. DOI: 10.1016/j.physe.2019.113580.

[29] Zhang Y Q, Wang L F, Jiang J N. Thermal vibration of rectangular single-layered black phosphorus predicted by orthotropic plate model[J]. *Journal of Applied Physics*, 2018, **123**: 095101. DOI: 10.1063/1.5016374.

[30] Yi J P, Wang L F, Zhang Y Q. Vibration of two-dimensional hexagonal boron nitride[J]. *Theoretical and Applied Mechanics Letters*, 2018, **8**(6): 408 − 414. DOI: 10.1016/j.taml.2018.06.003.

[31] Zhang Y Q, Wang L F. Thermal vibration of circular single-layered MoS_2 predicted by the circular Mindlin plate model[J]. *AIP Advances*, 2021, **11**(2): 025328. DOI: 10.1063/5.0038066.

[32] Jiang J W. Misfit strain induced buckling for transition-metal dichalcogenide lateral heterostructures: A molecular dynamics study[J]. *Acta Mech Solida Sinica*, 2019, **32**: 17 − 28. DOI: 10.1007/s10338-018-0049-z.

[33] Plimpton S. Fast parallel algorithms for short-range molecular dynamics[J]. *J Comput Phys*, 1995, **117**(1): 1 − 19. DOI: 10.1006/jcph.1995.1039.

[34] Peelaers H, van de Walle C G. Elastic constants and pressure-induced effects in MoS_2 [J]. *The Journal of Physical Chemistry C*, 2014, **118**(22): 12073 − 12076. DOI: 10.1021/jp503683h.

[35] Kandemir1 A, Yapicioglu H, Kinaci A, et al. Thermal transport properties of MoS_2 and $MoSe_2$ monolayers[J]. *Nanotechnology*, 2016, **27**(5): 055703. DOI: 10.1088/

0957-4484/27/5/055703.
[36] Vora A M. Effect of indium intercalation on various properties of $MoSe_2$ single crystals[J]. *Cryst Res Technol*, 2007, **42**(3): 286－289. DOI: 10.1002/crat.200610814.
[37] Hashemi Z, Rafiezadeh S, Hafizi R, et al. First-principles study of MoS_2 and $MoSe_2$ nanoclusters in the framework of evolutionary algorithm and density functional theory[J]. *Chemical Physics Letters*, 2018, **698**: 41－50. DOI: 10.1016/j.cplett.2018.03.008.
[38] Xiong Q L, Zhou J, Zhang J, et al. Spontaneous curling of freestanding Janus monolayer transition-metal dichalcogenides[J]. *Phys Chem Chem Phys*, 2018, **20**(32): 20988－20995. DOI: 10.1039/C8CP02011F.
[39] Ye H, Zhang Y Z, Wei A R, et al. Intrinsic-strain-induced curling of free-standing two-dimensional Janus MoSSe quantum dots[J]. *Applied Surface Science*, 2020, **519**: 146251. DOI: 10.1016/j.apsusc.2020.146251.

圆形 Janus 硫硒化钼板的振动行为分析

刘鑫杰　王立峰

(南京航空航天大学航空航天结构力学及控制全国重点实验室,南京 210016)

摘要:采用分子动力学(MD)模拟和有限元方法(FEM)研究了单层 Janus 硫硒化钼(MoSSe)的振动行为. 将晶格失配引起的固有应变添加到双层板模型中, 利用 FEM 实现了对 MoSSe 的模拟. 利用 MD 模拟和 FEM 计算出自由边界和固支边界下 MoSSe 圆板的振动情况,并分析了尺寸、应变和压力对固有频率的影响. 结果表明,自由边界下 MoSSe 圆板的固有频率随着尺寸的增加而逐渐减小. 当圆板直径达到 8.6 nm 时,频率出现明显的不连续现象,究其原因在于碗状翘曲和管状翘曲. 不同尺寸 MoSSe 圆板的固有频率的 MD 模拟结果与 FEM 计算结果一致,且在小变形情况下,2 种方法得到的应变与压力对固有频率的影响也一致. 双层板模型可以准确预测 MoSSe 板的振动行为.

关键词:单层 Janus 硫硒化钼(MoSSe); 分子动力学(MD); 翘曲; 固有频率
中图分类号:O327